Natural Frequencies and Damping Ratios of Multi-layered Laminated Glass Beams using a Dynamic Effective Thickness

F. Pelayo, López-Aenlle M.

Department of Construction and Manufacturing Engineering, University of Oviedo, Campus de Gijón, Zona Oeste, Edificio 7, 33203, Gijón, Spain.

*corresponding author; E-mail: fernandezpelayo@uniovi.es

Phone: +34985 181932

Abstract

Multi-layered laminated glass panels are those with at least three monolithic glass layers and two viscoelastic interlayers. Multi-layered laminated glass panels are commonly used in floors, roofs and other horizontal glazing accessible to the public where a high level of security is required. Although the glass can be consider a linear-elastic material, the viscoelastic interlayers determine a non-linear behavior of the laminated structure that must be taken into consideration. In this paper, a dynamic effective thickness is proposed to predict the natural frequencies and damping ratios of multi-layered laminated glass

beam-like structures with different boundary conditions and at different temperatures. Furthermore, the presented dynamic effective thickness can be also used to any frequency domain calculations such as displacements and stresses.

To validate the proposed model, operational modal analysis was carried out on a multi-layered laminated glass beam to obtain the experimental natural frequencies and damping ratios at 20, 25, 30 and 35 ^{o}C. Moreover, a finite element model of the beam was also assembly for the sake of comparison. The proposed model predicts the natural frequencies with errors less than 5% whereas the discrepancies in damping ratios are less than 50%.

Keywords

Multi-layered; laminated glass; viscoelastic behaviour; modal analysis; modal parameters; effective thickness concept

Abbreviations

E_{eff}	Effective Young modulus
E	Young's modulus of glass
$G_t(t)$	Viscoelastic relaxation shear modulus for the polymeric interlayer
H_i	Thickness of the i-th glass layer in laminated glass
t_i	Thickness of the i-th polymeric layer in laminated glass

$K_t(t)$	Viscoelastic bulk modulus of the interlayer
L	Length of a glass beam
T	Temperature
T_0	Reference temperature

Lowercase letters

a_T	Shift factor
b	Width of a glass beam
$g(x)$	Shape function (Galuppi and Royer Carfagni model)
t	Time
w	Deflection

Greek letters

ρ_t	Density of the polymeric interlayers
ρ_G	Density of the glass layers

Introduction

Laminated glass beams are sandwich elements which show a viscoelastic behavior [1, 2, 3 and 4]. A typical laminated glass panel consist of two outer monolithic glass layers and

one interlayer of a polymer (figure 1) such as polyvinyl butyral (PVB). The polymer interlayers work in a wide range of temperatures due, i.e. to the seasonally changing weather conditions.

Multi-layered laminated glass panels (figure 1) are those with at least three monolithic glass layers and two viscoelastic interlayers [5, 6]. Multi-layered laminated glass panels can be used for many different applications due to the added thickness and strength as well as the high damping exhibited by these elements and they are also subject to different types of loading (permanent, variable, impact, etc.). The glass may be annealed, heat or chemically strengthened or fully tempered [7, 8].

Multi-layered laminated glass panels are commonly used in accessible glazing, i.e. floors, roofs and other horizontal glazing accessible to the public or, at least, for cleaning and maintenance [8]. In these applications must be examined, among others, resistance against impact caused by a hard or soft body, the post-breakage behavior as well as the slip resistance [8]. Multi-layered laminated glass panels are mandatory in some codes and standards. According to DIN 18008-5 [9], glass floor panels must consist of at least three glass layers with PVB interlayers and the uppermost glass layer must be neglected for structural analysis. With respect to code ÖNORM B3716 [10] the load carrying layer must be of laminated glass with and additional abrasion layer and thermally toughened glass is only allowed in combination with float or strengthened glass and the minimal thickness of the PVB layers is 0.76 mm [7].

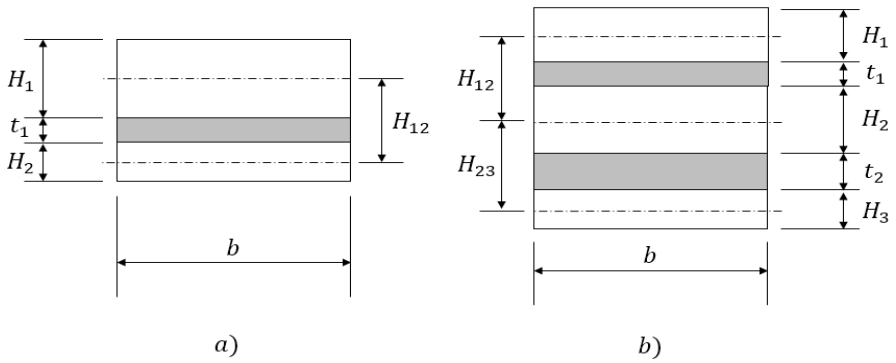

Figure 1. Section of a sandwich (a) and a multi-layered (b) glass beam.

Glass walkways are another application of multi-layered laminated glass. The standard ASTM 2751-11 [11] (Practice for the Design and Performance of Supported Glass Walkways) contains calculation and testing methods applicable to the design of glass walkways constructed with laminated glass including interior and exterior walking surfaces constructed and intended for pedestrian use (floors, ramps, sidewalks, and stair treads). The Grand Canyon glass walkway was built with a 40 mm thick quadruple laminate consisting of heat strengthened glass and one fully tempered glass (lower supported ply). The additional upper 8 mm tempered ply was ignored in the analysis and provides additional safety and redundancy [6].

Glass mechanical behavior is usually modeled as linear-elastic whereas the PVB shows linear-viscoelastic behavior. A fundamental characteristic of viscoelastic materials is that the mechanical properties are frequency (or time) and temperature dependent [12, 13, 14, 15]. The mechanical behavior of laminated glass is not elastic and the sections do not

behave according to the Euler-Bernoulli Beam theory assumptions (plane sections remain plane) due to the shear effect of the interlayers [1, 2].

Some analytical models proposed for laminated glass elements [16] simplify the calculation considering the polymeric interlayer as a linear elastic material where the shear modulus is chosen according to the temperature and load duration, i.e., neglecting the "memory effect" of viscoelasticity. Galuppi and Royer-Carfagni [1] concluded that a full viscoelastic analysis is only recommended when one is interested in a precise design of a laminated glass structures. Bennisson et al. [3, 4] proposed the concept of effective thickness for simplifying calculations of laminated glass elements under static loading, based on a previous work developed by Wölfel [17]. The method consists of calculating the thickness of a monolithic beam with equivalent bending properties to a laminated beam. The effective thickness can then be used in analytical equations and simplified finite element models in place of the actual thickness of the laminated glass beam [1, 2, 3, 4, 18 and 19]. This methodology has also been extended to the two-dimensional case (laminated plates) under various loads and boundary conditions [20] and to the case of multi-layered laminated glass beams [5].

With regard to the dynamic behavior, Ross, Kerwin and Ungar were the first to study the flexural vibration of a sandwich configuration [21, 22] and they proposed an effective complex flexural stiffness which can be used to determine the modal parameters of a sandwich beam using the equations and the wavenumbers corresponding to an Euler-

Bernoulli beam. They assumed that the wave motion in a constrained layer configuration can be described by a fourth-order differential equation. Ditaranto [23, 24] and Mead and Markus [25, 26] demonstrated that the flexural motion of a sandwich beam is governed by a sixth-order linear homogeneous differential equation.

Aenlle and Pelayo [18] proposed a dynamic effective thickness for calculating modal parameters in laminated glass beams using simple monolithic elastic models. This method was extended by the same authors to laminated glass plates in [19].

With respect to numerical simulations, many papers and books have been published about the modelling of sandwich and laminated elements [19, 20, 27, 28, 29, 30, 31, 32] subject to static and dynamic loadings. Galuppi and Royer Carfagni [20] proposed an analytical model to calculate the static response of laminated glass elements and the predictions are validated by numerical simulations. In [27, 28] the iso-geometric analysis, the level set and a simple-first order shear deformation theory are combined to simulate more effectively the free vibration of laminated composite plates. In [29, 30, 31] meshfree methods are developed for free and forced vibration analysis of 2D elements. The basis functions for the CQ4 (4-node quadrilateral element) element are used to analyze the free and forced 2D vibrations of linear elastic and piezoelectric structures [32].

In this paper, the effective thickness developed by Galuppi and Royer Carfagni [5] to calculate deflections in multi-layered laminated glass beams under static loadings is here extended to the frequency domain using the correspondence principle [13, 14, 33, 34]. Furthermore, a dynamic effective thickness is also derived solving the differential equation of flexural wave motion. In order to validate the model, the modal parameters of a multi-layered laminated glass beam consisting of three annealed glass layers and two PVB interlayers were estimated by operational modal analysis at different temperatures in the range 20-35ºC. The experimental results are compared with the predictions provided by the proposed analytical model and with the results obtained with a finite element model assembled in ABAQUS [35].

State of the art

Static deflection effective thickness in laminated glass beams

Galuppi and Royer-Carfagni [2] derived an analytical expression for the deflection effective thickness of a laminated glass beam composed of two glass layers and one polymeric interlayer using a variational approach. In their work, the following assumptions were considered: the face plates are purely elastic, the core is linearly viscoelastic with shear modulus G_t (t, T), the shear strains in the face plates are negligible, the longitudinal stresses in the core are negligible, there is no slipping between the elastic and viscoelastic layers at their interfaces and the three layers have the same transversal

displacement $w(x,t,T)$. Moreover, the authors also assume that the deflection shape of the laminated glass beam coincide with that of a monolithic beam with the same loading and boundary conditions, i.e., the deflection of the beam is expressed as:

$$w(x,t,T) = -\frac{g(x)}{EI(t,T)_{S2}} \tag{1}$$

where g(x) is a shape function that takes the form of the elastic deflection of a monolithic beam with constant cross section under the same loading and boundary conditions as the laminated glass beam and $EI(t,T)_{S2}$ is the bending stiffness of the laminated glass beam given by:

$$\mathrm{EI(t,T)}_{s2} = \frac{1}{\frac{\eta_{S2}(\mathrm{t,T})}{\mathrm{EI_{TOT2}}} + \frac{1-\eta_{S2}(\mathrm{t,T})}{\mathrm{EI_{T2}}}} \tag{2}$$

Where:

- subindex "s" indicates static
- subindex "2" indicates beam with two glass layers and one interlayer
- $I_{T2} = I_1 + I_2 = b\frac{H_1^3+H_2^3}{12}$
- $I_{TOT2} = I_{T2} + A_1 d_1^2 + A_2 d_2^2$
- $d_1 = \frac{H_2 H_{12}}{H_1+H_2}$
- $d_2 = -\frac{H_1 H_{12}}{H_1+H_2}$

- $H_{12} = t_1 + \left(\frac{H_1+H_2}{2}\right)$
- The parameter $\eta_{S2}(t, T)$ is given by :

$$\eta_{S2}(t,T) = \frac{1}{1 + \frac{EI_{T2}\,(A_1 d_1^2 + A_2 d_2^2)\psi_B}{b\mathrm{G_t}(t,T) I_{TOT2}\left(\frac{H_{12}^2}{t_1}\right)}} \tag{3}$$

- ψ_B is a constant parameter which depends on the boundary and loading conditions [2] and it is given by:

$$\psi_B = \frac{\int_0^L \left(g''(x)\right)^2 dx}{\int_0^L \left(g'(x)\right)^2 dx} \tag{4}$$

Using the dimensionless standard geometric parameter Y_{B2}:

$$Y_{B2} = \frac{EI_{TOT2}}{\mathrm{EI_{T2}}} - 1 = \frac{(A_1 d_1^2 + A_2 d_2^2)}{I_{T2}} = \frac{bH_{12}^2 H_1 H_2}{I_{T2}(H_1+H_2)} \tag{5}$$

and the dimensionless shear parameter $g_2(t, T)$ commonly used in sandwich beams [25, 26 and 36] which defines the shear coupling between the core and outer layers:

$$g_{S2}(t,T) = \frac{G_t(t,T)L^2(H_1+H_2)}{EtH_1H_2} = \frac{G_t(t,T)}{E}\frac{H_{12}^2}{t}\frac{bL^2}{I_{T2}Y_{B2}} \tag{6}$$

Eq. (2) can be expressed as:

$$EI(t,T)_{S2} = EI_{T2}\left(1 + \frac{Y_{B2}}{1 + \frac{\psi_B L^2}{g_{S2}(t,T)}}\right) \tag{7}$$

If the shear modulus is constant $G_t(t,T) = G_t$, the shear parameter is also constant and it is given by:

$$g_{E2} = \frac{G_t L^2 (H_1 + H_2)}{E t H_1 H_2} = \frac{G_t}{E}\frac{H_{12}^2}{t}\frac{bL^2}{I_{T2} Y_{B2}} \tag{8}$$

If Eq. (8) is substituted in Eq. (7), the later becomes:

$$EI_{E2} = EI_{T2}\left(1 + \frac{Y_{B2}}{1 + \frac{\psi_B L^2}{g_{E2}(t,T)}}\right) \tag{9}$$

Which is also constant and it represents the stiffness of the sandwich beam when both the core and the glass layers show a linear-elastic behavior.

In the case of three glass layers of equal thickness H and two polymeric interlayers with thickness t, the static flexural stiffness can be derived from [5] and it is given:

$$EI(t,T)_{S3} = EI_{T3}\left(1 + \frac{Y_{B3}}{1 + \frac{\psi_B L^2}{g_{S3}(t,T)}}\right) \quad (10)$$

Where:

- subindex "3" indicates beam with 3 glass layers
- $I_{T3} = 3I = 3\frac{bH^3}{12}$
- $Y_{B3} = \frac{8(t+H)^2}{H^2}$
- $g_{S3}(t,T) = \frac{G_t(t,T)}{E\,Ht}$ (11)
- ψ_B is a constant parameter which takes the same values as those derived for the beam with 2 glass layers [2].

If the case that the shear modulus is constant $G_t(t,T) = G_t$, the elastic shear parameter is given by:

$$g_{E3} = \frac{G_t}{E\,Ht} \quad (12)$$

Whereas the elastic flexural stiffness is expressed as:

$$EI_{E3} = b\frac{H^3}{4}\left(1 + \frac{Y_{B3}}{1 + \frac{\psi_B L^2}{g_{E3}}}\right) \tag{13}$$

Dynamic effective thickness in sandwich glass beams

Mead and Markus (M&M) [25, 26] derived a sixth-order differential equation that governs the flexural wave motion of a three layered constrained-layer damping beam when it vibrates freely at frequency ω . The differential equation is given by:

$$EI_{T2}\left(w^{VI}(x,t,T) - g_{d2}^{*}(\omega,T)\ (1 + Y_{B2})\, w^{IV}(x,t,T)\right) -$$

$$-\omega^2\, \bar{m}_2\left(w^{II}(x,t,T) - g_{d2}^{*}(\omega,T)\ w(x,t,T)\right) = 0 \tag{14}$$

Where the roman numerals superscripts denote differentiation with respect to x, the superscript "*" indicates complex, the subscript "d" indicates dynamic, $\bar{m}_2$ is the mass per unit length of the beam, i.e.:

$$\bar{m}_2 = b\rho_G(H_1 + H_2) + b\rho_t t_1 \tag{15}$$

and $g_{d2}^{*}(\omega,T)$ is the shear parameter given by:

$$g_{d2}^{*}(\omega,T)=\frac{G_t^{*}(\omega,T)\,L^2}{Et}\left(\frac{H_1+H_2}{H_1H_2}\right)=\frac{G_{t(\omega,T)}^{*}}{E}\,\frac{H_{12}^2}{t}\frac{bL^2}{I_{T2}Y_{B2}} \tag{16}$$

Eq. (10) yields the following polynomial equation for $k^{*}L$:

$$(k^{*}L)^6-g_{d2}^{*}(\omega,T)\,(1+Y_{B2})(k^{*}L)^4-\Omega^{*2}(k^{*}L)^2+\Omega^{*2}g_{d2}^{*}(\omega,T)=0 \tag{17}$$

where k^{*} is a complex wavenumber:

$$k^{*}=k_R+i\cdot k_I \tag{18}$$

and Ω^{*} is a non-dimensional frequency defined by [25, 26]:

$$\Omega^{*2}=\frac{\omega^{*2}\,\overline{m_2}\,L^4}{EI_{T2}} \tag{19}$$

Eq. (19) after rearrangement yields to:

$$\Omega^{*2}=(k^{*}L)^4\left(\frac{(k^{*}L)^2-g_{d2}^{*}(\omega,T)(1+Y_{B2})}{(k^{*}L)^2-g_{d2}^{*}(\omega,T)}\right) \tag{20}$$

or:

$$\omega^{*2}=\omega^2(1+i\cdot\eta)=\frac{k*^4}{\overline{m}_2}EI_{T2}\left(1+\frac{Y_{B2}}{1-\dfrac{k^{*2}\,L^2}{g_{d2}^{*}(\omega,T)}}\right) \tag{21}$$

If the real part of k^* is neglected, i.e., $k_R = 0$, k^* is given by $k^* = i \cdot k_I$ and Eq. (21) results in:

$$\omega^2(1 + i \cdot \eta) = \frac{k_I^4}{\overline{m}_2} EI_{T2} \left(1 + \frac{Y_{B2}}{1 + \frac{k_I^2 L^2}{g_{d2}^*(\omega, T)}} \right) \tag{22}$$

From Eq. (22) the following equation for the effective complex flexural stiffness can be defined:

$$EI^*(\omega, T)_2 = EI_{T2} \left(1 + \frac{Y_{B2}}{1 + \frac{k_I^2}{g_{d2}^*(\omega, T)}} \right) \tag{23}$$

Which can be used to estimate modal parameters, displacements and stresses in laminated glass beams [19, 37]. In the case of a simply supported beam, the wavenumber is given by:

$$k_I = n \frac{\pi}{L} \tag{24}$$

With 'n' being the order of the mode and the stiffness given by Eq. (23) coincides with that derived by Ross, Kerwin, and Ungar [21, 22] considering the beam simply supported and vibrating at a natural frequency, which means that the flexural deformation of the beam during vibration is spatially sinusoidal in shape. Later, the effective complex flexural stiffness was extended to other boundary conditions using the appropriate wavenumbers [12, 22].

From Eqs. (7) and (23) it is inferred that the square of the wavenumber k_I^2 and the shear parameter $g_{d2}^*(\omega, T)$ play in dynamics the same role as the parameters ψ_B and $g_{S2}(t, T)$, respectively, in statics.

Moreover, the effective complex flexural stiffness $\mathrm{EI}^*(\omega, \mathrm{T})_2$ can be easily derived from the elastic stiffness $\mathrm{EI}_{\mathrm{E2}}$ (Eq. (9)) applying the correspondence principle. With respect to the shear parameter $\mathrm{g}_{\mathrm{d2}}^*(\omega, \mathrm{T})$ it can also be derived from the elastic shear parameter g_{E2} (Eq. (8)) applying the correspondence principle but with the special feature that the wavenumber k_I^2 must be used instead of parameter ψ_B [38].

Dynamic effective thickness of a symmetric three glass multi-layered beam

In this section an expression for the effective complex flexural stiffness of a laminated glass beam composed of three glass layers of equal thickness and two polymeric

interlayers is derived. This expression can be formulated solving the differential equation that governs the flexural wave motion of a multi-layered glass beam or alternatively applying the correspondence principle to the stiffness of a laminated glass beam with both the core and the glass layers showing a linear-elastic behavior.

Dynamic effective thickness by the correspondence principle

The correspondence principle [13, 14, 33, 34] states that if a solution to a linear elasticity problem is known, the solution to the corresponding problem for a linearly viscoelastic material can be obtained by replacing each quantity which can depend on time by its Fourier Transform. In order that the elastic and viscoelastic solutions correspond, the interface between boundary regions under specified displacement and under specified stress must not change with time.

In order to apply the correspondence principle, an elasticity solution must be known [34]. Wherever an elastic constant appears, it is replaced with the corresponding complex dynamic viscoelastic function. Some examples of application are shown in Table 1.

Table 1. Examples of application of the correspondence principle (superscript '*' indicates complex).

	Constitutive equation	Bending	Natural frequencies

Linear-Elastic	$\sigma = E \cdot \epsilon$	$\sigma = \frac{M}{EI}$	$\omega^2 = k^4 \frac{EI}{\rho A}$
Linear-Viscoelastic	$\sigma(\omega) = E^*(\omega) \cdot \epsilon(\omega)$	$\sigma(\omega) = \frac{M(\omega)}{E^*(\omega)I}$	$\omega^{*2} = k^{*4} \frac{E^*(\omega)I}{\rho A}$

For a laminated glass beam with three glass layers of equal thickness H and two polymeric interlayers of equal thickness t, the effective complex flexural stiffness can be derived applying the correspondence principle to Eq. (13), i.e.:

$$EI^*(\omega,T)_3 = b\frac{H^3}{4}\left(1+\frac{Y_{B3}}{1+\frac{k_I^2}{g_{d3}^*(\omega,T)}}\right) \tag{25}$$

With respect to parameter$g_{d3}^*(\omega,T)$, it is given by:

$$g_{d3}^*(\omega,T) = \frac{G_t^*(\omega,T)}{E\,Ht} \tag{26}$$

which can also be derived from Eq. (12) applying the correspondence principle.

The natural frequencies and damping ratios can be now obtained by:

$$\omega^2(1+i\cdot\eta) = \frac{k_I^4}{\overline{m}_3} EI^*(\omega,T)_3 \tag{27}$$

Where:

$$\overline{m}_3 = 3b\rho_G H + 2\rho_t bt \tag{28}$$

is the mass per unit length of the beam.

Dynamic effective thickness by solving the flexural wave motion differential equation

The effective complex flexural stiffness (Eq. (25)) can also be formulated from the equation of motion corresponding to the beam vibrating freely at frequency ω which is given by [39]:

$$EI_{T3}\left(w^{VI}(x,t,T) - g^*_{d3}(\omega,T)\ (1+Y_{B3})\, w^{IV}(x,t,T)\right) -$$

$$-\omega^2\, \overline{m}_3\left(w^{II}(x,t,T) - g^*_{d3}(\omega,T)\ w(x,t,T)\right) = 0 \tag{29}$$

Eq. (29) yields the following polynomial equation for k^*L:

$$(k^*L)^6 - g^*_{d3}(\omega,T)\,(1+Y_{B3})(k^*L)^4 - \frac{\omega^{*2}\,\overline{m_3}\,L^4}{EI_{T3}}(k^*L)^2 - g^*_{d3}(\omega,T) = 0 \tag{30}$$

From which:

$$\omega^{*2} = (k^*L)^4\,\frac{EI_{T3}}{\overline{m_3}\,L^4}\left(\frac{(k^*L)^2 - g^*_{d3}(\omega,T)(1+Y_{B3})}{(k^*L)^2 - g^*_{d3}(\omega,T)}\right) \tag{31}$$

Neglecting the real part of the wavenumber, i.e. $k^* = i \cdot k_I$, the following equation for the complex flexural effective stiffness corresponding to a symmetric laminated glass beams with 3 glass layers of equal thickness H and 2 polymeric interlayers of equal thickness t is inferred:

$$EI^*(\omega,T)_3 = b\frac{H^3}{4}\left(1+\frac{Y_{B3}}{1+\frac{k_I^2}{g_{d3}^*(\omega,T)}}\right) \tag{32}$$

Which coincides with Eq. (25) derived applying the correspondence principle.

Finally, expressions for the dynamic effective thickness and the dynamic effective Young modulus [18, 19, 37 and 38] can be derived from the complex flexural effective stiffness (Eqs. (25) or (32)). If a monolithic model with constant thickness H_T :

$$H_T = 3H + 2t \tag{33}$$

is going to be used to calculate modal parameters, displacements or stresses in the frequency domain, a dynamic effective Young modulus (Young modulus of a monolithic beam which provides the same modal parameters as the laminated one) can derived from:

$$E_{eff}(\omega,T)_3\frac{bH_T^3}{12} = EI^*(\omega,T)_3 \tag{34}$$

Which leads to:

$$E^*_{eff}(\omega,T)_3 = \frac{3H^3}{H_T^3}\left(1+\frac{Y_{B3}}{1+\frac{k_I^2L^2}{g^*_{d3}(\omega,T)}}\right) \tag{35}$$

On the other hand, a dynamic effective thickness can be formulated from:

$$\frac{EH^{*3}_{eff}(\omega,T)}{12} = EI^*(\omega,T)_3 \tag{36}$$

Which results in:

$$H_{eff3}(\omega,T) = \sqrt[3]{3H^3\left(1+\frac{Y_{B3}}{1+\frac{k_I^2L^2}{g^*_{d3}(\omega,T)}}\right)} \tag{37}$$

Any of the three dynamic effective parameters proposed: complex flexural stiffness, thickness and Young modulus, can be used for predicting the dynamic response of a multi-layered beam as well as to calculate other variables in the frequency domain such as displacements or stresses.

Numerical and experimental validation

In this paper the modal parameters of a multi-layered glass beam composed of three annealed glass layers and two polymeric interlayers made of polyvinyl butyral (PVB) were predicted with Eq. (27) using the dynamic effective thickness given by Eq. (25). The analytical predictions were validated with experimental tests and numerical simulations. The multi-layered beam used in this work presents the following geometrical data (see figure 1): $L = 1.40$ m, $H_1 = H_2 = H_3 = 4$ mm, $t_1 = t_2 = 0.76$ mm and $b = 100\ mm$.

The material properties presented in Table 2 were considered for the glass and PVB layers. With respect to PVB, its mechanical properties were obtained in a previous work [18] by a viscoelastic characterization carried out in a DMA RSA3 (T.A. Instruments). The Prony series for the shear relaxation modulus $G_t(t,T)$ is given by:

$$G_t(t) = G_0 \cdot \left[1 - \sum_{i=1}^{n} g_i \cdot \left(1 - \exp\left(\frac{-t}{\tau_i}\right)\right)\right] \tag{38}$$

where the parameters g_i and τ_i are shown in Table 3.

Moreover, the effect of temperature was considered using the William, Landel and Ferry (WLF) model [40] where the TTS (Time Temperature Supersposition) shift factor, a_T, is given by:

$$\log(a_T) = -C_1 \frac{(T - T_0)}{C_2 + (T - T_0)} \tag{39}$$

The coefficients C_1 and C_2 are shown in Table 2. Once the shift factor a_T is determined for a specific temperature T, the shear relaxation modulus for this temperature $G_t(t, T)$ can be obtained from the relation:

$$\mathrm{G(t, T)} = a_T \, G(t, T_0) \tag{40}$$

where $G(t, T_0)$ is known as the master curve of the viscoelastic material at reference temperature T_0.

Table 2. Material properties for glass and PVB.

Glass			PVB					
E (Young's Modulus) [GPa]	ν (Poisson's ratio)	ρ (Density) [kg/m^3]	G_0 (Instantaneous shear modulus) [GPa]	K (Bulk Modulus) [GPa]	ν (Poisson's ratio)	ρ (Density) [kg/m^3]	C_1 (WLF: Tref=20C)	C_2 (WLF: Tref=20C)
70	0.22	2500	0.3696	2	0.40	1046	12.60	74.46

Table 3. Prony series coefficients for PVB.

Term	g_i	τ_i [s]
1	2.342151953E-01	2.36600000000000E-07
2	2.137793134E-01	2.26430000000000E-06
3	1.745500419E-01	2.16668000000000E-05
4	1.195345045E-01	2.07327300000000E-04
5	1.362133454E-01	1.98389580000000E-03

6	6.840656310E-02	1.89837195000000E-02
7	4.143944180E-02	1.81653498300000E-01
8	7.251952800E-03	1.73822593210000E+00
9	2.825459600E-03	1.66329270788000E+01
10	2.712854000E-04	1.59158978189400E+02
11	4.293523000E-04	1.52297789909670E+03
12	9.804730000E-05	1.45732380763177E+04
13	5.274937000E-04	1.39449999999999E+05

Analytical predictions

The natural frequencies and the damping ratios for the first four modes of the beam in the temperature range 10^oC to 40^oC were predicted using Eq. (27) and the dynamic complex effective stiffness given by Eq. (25). The wavenumbers needed in Eq. (27) were considered equal to those of a monolithic beam with the same boundary conditions. The analytical predictions for the simply supported and free-free boundary conditions are presented in figures from 6 to 13. The predicted values corresponding to temperatures: $20^oC, 25^oC, 30^o$ and 35^oC are shown in Tables 4 and 5, respectively. It can be observed that the natural frequencies decrease with increasing temperature. This tendency is expected because the shear modulus of the PVB also decreases with increasing temperature. With respect to damping, it increases with increasing temperature. In this paper it has been considered that the loss factor η and the modal damping ζ are related by [41, 42]:

$$\eta \cong 2\,\zeta \tag{41}$$

Numerical simulations

A 3D finite element model was assembled in ABAQUS using the same geometrical data and material properties (see Table 2 and 3) as those considered in the analytical predictions. 3D linear shell continuum elements (SC8R) were used for the glass layers [35] whereas the PVB layers were meshed with 3D linear hexahedral elements (C3D8R). This meshing technique has been demonstrated to be adequate to reproduce the laminated glass behavior with a relatively low computational time [43]. A detail of the mesh is shown in figure 2.

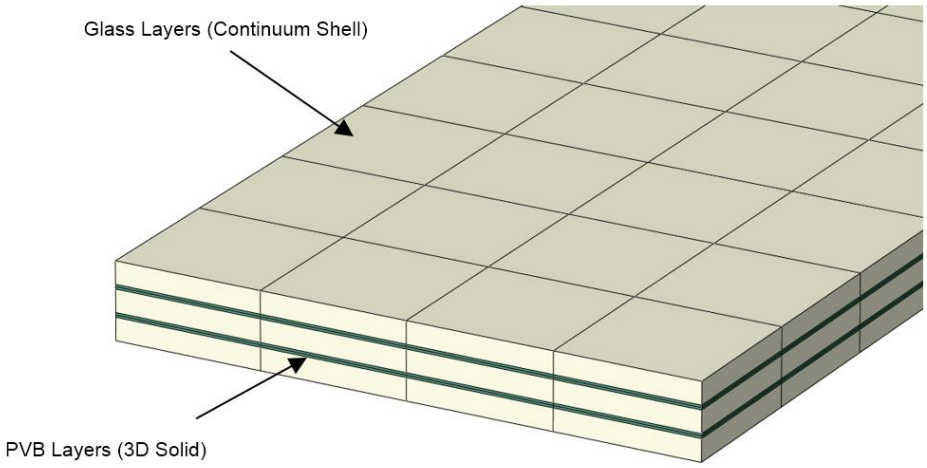

Figure 2. Detail of the beam mesh.

The numerical frequency response function (FRF) was obtained from a sweep sine analysis (linear frequency analysis) [35] subjecting the specimen to a uniform loading with a magnitude of 1 N for all the frequency range considered in the simulations. Both free-free and simply-supported boundary conditions were simulated. Then, the natural frequencies were estimated by the peak picking method [41, 42] (figure 3) whereas the damping ratios were obtained by the logarithmic decrement technique [41, 42] (figure 3). The numerical natural frequencies and damping ratios are presented in tables 4 and 5, respectively.

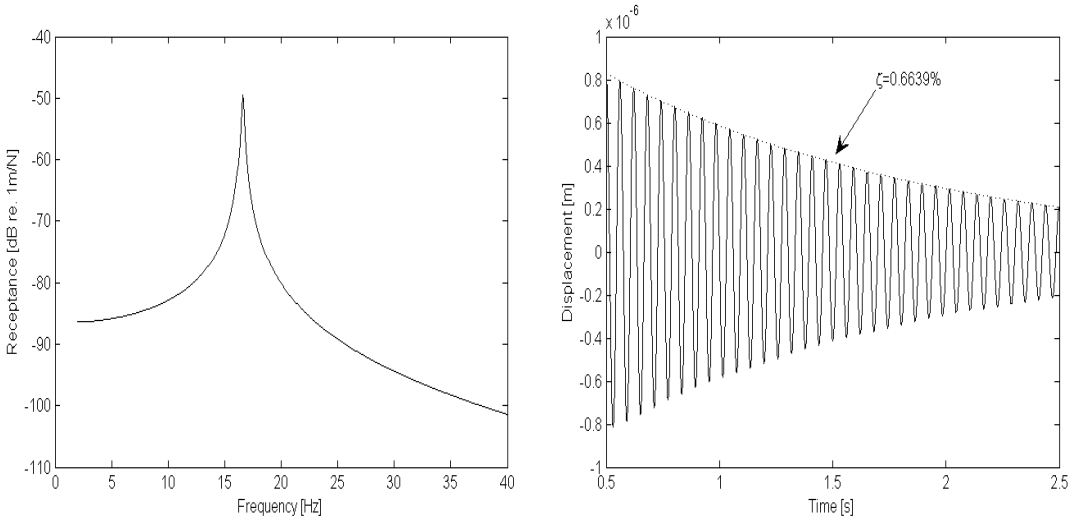

Figure 3. Zoom of the receptance (left) and its corresponding free decay (right) for the 1st mode with the beam simply-supported at 20 ºC.

Experimental results

The modal parameters of the beam were also experimentally determined by operational modal analysis. The responses of the beam were measured using 7 accelerometers with a sensitivity of 100 mV/g, uniformly distributed (figure 4) and recorded with a 16 channels TEAC LX-120 data acquisition system. The arrows in figure 4 show the location and the direction of the sensors. The beam was excited applying small hits randomly along its length with an impact hammer and the responses were recorded for approximately 4 minutes using a sampling frequency of 1000 Hz. The modal tests were performed in a chamber-oven at $20, 25, 30$ and 35 ºC, respectively.

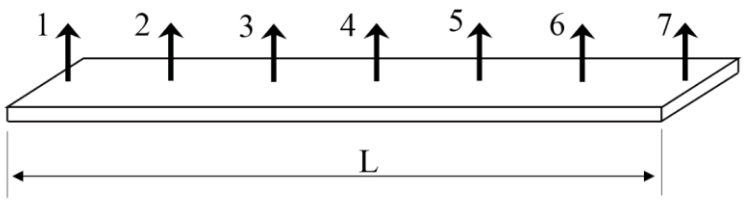

Figure 4. Test setup with the location of the accelerometers.

Figure 5 shows the singular value decomposition of the responses at 20^{o}C and 30ºC for the free-free boundary conditions. As temperature increases the peaks become less clear for the higher modes and only the modal parameters of first mode were accurately identified over 35ºC.

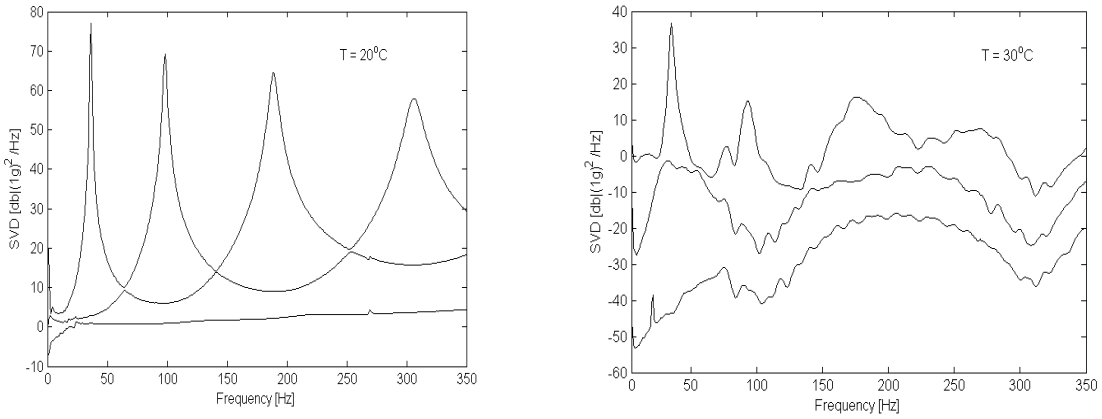

Figure 5. Singular value decomposition at 20 and 30ºC for the free-free conditions.

Modal parameters were estimated using both Frequency Domain Decomposition (EFDD) [44] and Stochastic Subspace iteration method (SSI) [45]. The experimental natural frequencies and damping ratios estimated with the EFDD technique are shown in tables 4 and 5, respectively. The SSI technique provides similar results and they are not presented in the paper.

Table 4. Analytical, numerical and experimental results for the free-free boundary conditions.

		Results						Errors					
Tª	Mode	Analytical		Numerical		Experimental		Analy.-Numeric.		Analy.-Exp.		Numeric.-Exp.	
		Freq. [Hz]	ζ [%]	Freq. [Hz]	ζ [%]	Freq. [Hz]	ζ [%]	Freq. [%]	ζ [%]	Freq. [%]	ζ [%]	Freq. [%]	ζ [%]
20ºC	1	37.25	0.84	36.58	0.63	36.14	0.59	1.81	24.92	2.98	30.30	1.19	7.16
	2	101.01	1.47	99.35	1.38	98.28	1.20	1.64	6.17	2.70	18.17	1.08	12.79
	3	193.55	1.95	191.18	1.86	188.94	1.62	1.22	4.53	2.38	16.74	1.17	12.78
	4	311.50	2.55	308.58	2.42	306.13	2.20	0.94	5.02	1.72	13.57	0.79	9.00
25ºC	1	36.97	1.45	36.39	1.01	35.95	1.16	1.57	30.25	2.76	19.85	1.21	14.91
	2	99.20	2.43	97.87	2.15	96.56	2.11	1.34	11.50	2.67	13.54	1.35	2.30
	3	188.61	3.71	186.80	3.56	185.52	2.92	0.96	3.97	1.64	21.43	0.69	18.19
	4	302.52	4.76	300.61	4.41	297.53	4.37	0.63	7.22	1.65	8.24	1.03	1.10
30ºC	1	36.26	3.34	35.95	2.22	35.40	3.14	0.86	33.56	2.39	6.14	1.54	41.28
	2	96.26	5.03	95.56	3.98	93.32	3.95	0.73	20.83	3.05	21.57	2.34	0.94
	3	180.67	6.36	180.02	5.73	175.72	5.41	0.36	9.89	2.74	15.01	2.39	5.69
	4	284.66	7.45	283.86	6.98	---	---	0.28	6.19	---	---	---	---
35ºC	1	34.77	7.09	35.13	4.48	33.62	7.94	1.04	36.80	3.31	12.02	4.30	77.23
	2	90.11	9.95	90.86	8.21	83.07	---	0.84	17.52	7.81	---	---	---
	3	165.37	12.15	166.87	---	---	---	0.91	---	---	---	---	---
	4	256.48	13.78	258.63	---	---	---	0.84	---	---	---	---	---

Table 5. Analytical, numerical and experimental results for the simply-supported boundary conditions.

		Results						Errors					
		Analytical		Numeric		Experimental		Analy.-Numeric		Analy.-Exp.		Numeric-Exp.	
Tª	Mode	Freq. [Hz]	ζ [%]	Freq. [Hz]	ζ [%]	Freq. [Hz]	ζ [%]	Freq. [%]	ζ [%]	Freq. [%]	ζ [%]	Freq. [%]	ζ [%]
20ºC	1	16.56	0.49	16.58	0.66	16.59	0.69	0.10	36.63	0.18	42.42	0.08	4.23
	2	65.23	1.20	65.43	1.44	67.05	1.46	0.31	19.90	2.79	21.89	2.47	1.66
	3	143.97	1.70	144.37	1.96	150.53	2.04	0.28	15.14	4.56	19.82	4.27	4.07
	4	249.57	2.23	250.08	2.47	251.95	3.22	0.20	10.82	0.95	44.39	0.75	30.30
25ºC	1	16.48	1.02	16.49	1.26	16.50	1.31	0.05	23.97	0.14	29.31	0.09	4.31
	2	64.43	1.89	64.58	2.18	65.68	2.25	0.24	15.45	1.94	19.15	1.69	3.21
	3	141.34	2.84	140.63	3.42	146.20	3.26	0.50	20.24	3.44	14.72	3.96	4.59
	4	242.74	4.29	242.59	4.58	---	---	0.06	6.82	---	---	---	---
30ºC	1	16.27	2.39	16.23	2.72	16.30	2.84	0.25	13.37	0.17	18.75	0.43	4.75
	2	62.85	4.22	62.68	4.74	64.35	4.62	0.28	12.35	2.38	9.50	2.66	2.54
	3	135.77	5.74	135.19	6.70	140.03	6.99	0.42	16.70	3.14	21.65	3.58	4.25
	4	230.55	6.92	229.06	7.99	---	---	0.65	15.51	---	---	---	---
35ºC	1	15.79	5.19	15.72	5.56	15.83	5.88	0.44	7.07	0.28	13.31	0.72	5.83
	2	59.54	8.64	59.12	9.19	59.94	---	0.70	6.42	0.66	---	1.37628	---
	3	125.60	11.12	124.31	11.79	---	---	1.02	6.0633	---	---	---	---
	4	209.17	13.04	205.95	13.69	---	---	1.54	5.0201	---	---	---	---

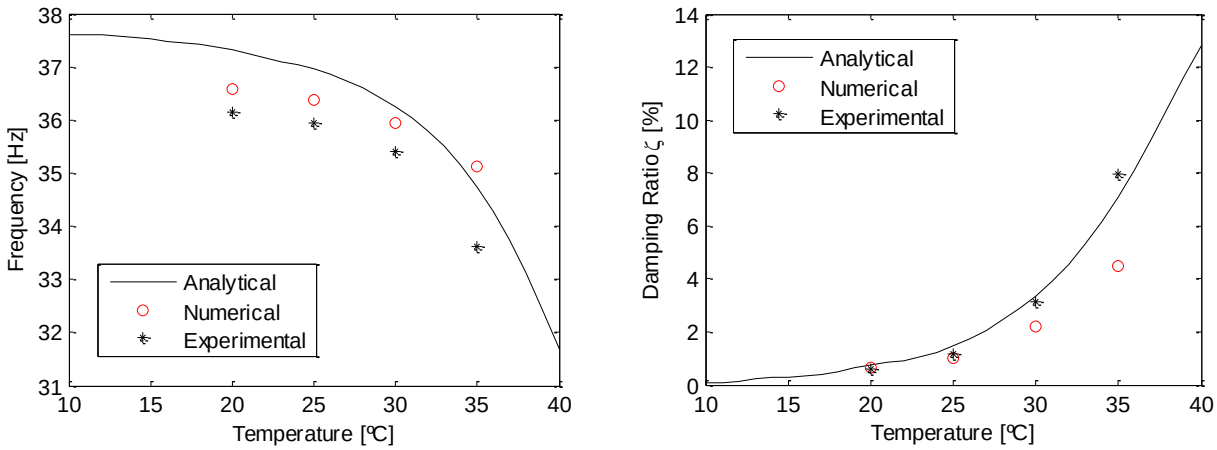

Figure 6. Analytical, numerical and experimental results for the free-free boundary conditions: Mode 1.

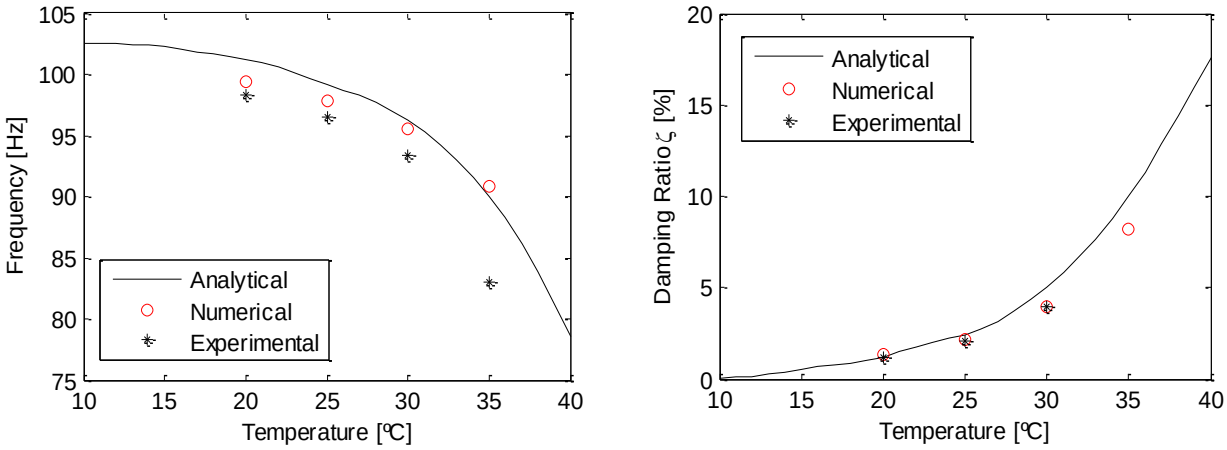

Figure 7. Analytical, numerical and experimental results for the free-free boundary conditions: Mode 2.

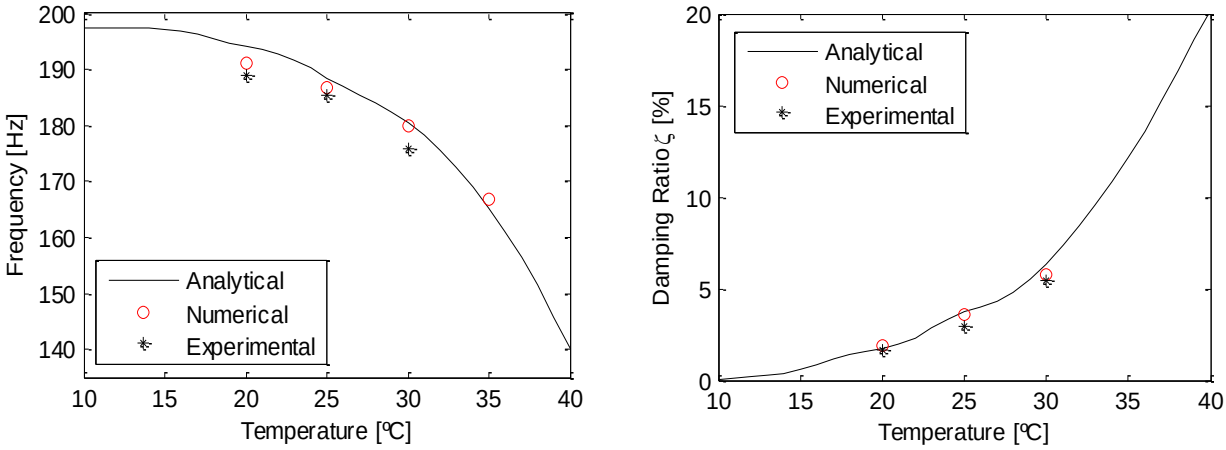

Figure 8. Analytical, numerical and experimental results for the free-free boundary conditions: Mode 3.

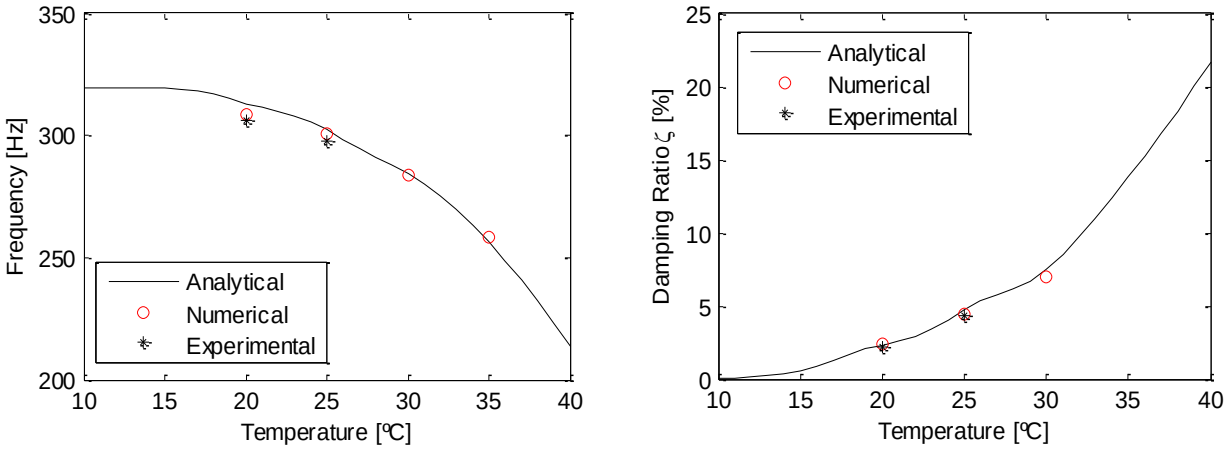

Figure 9. Analytical, numerical and experimental results for the free-free boundary conditions: Mode 4.

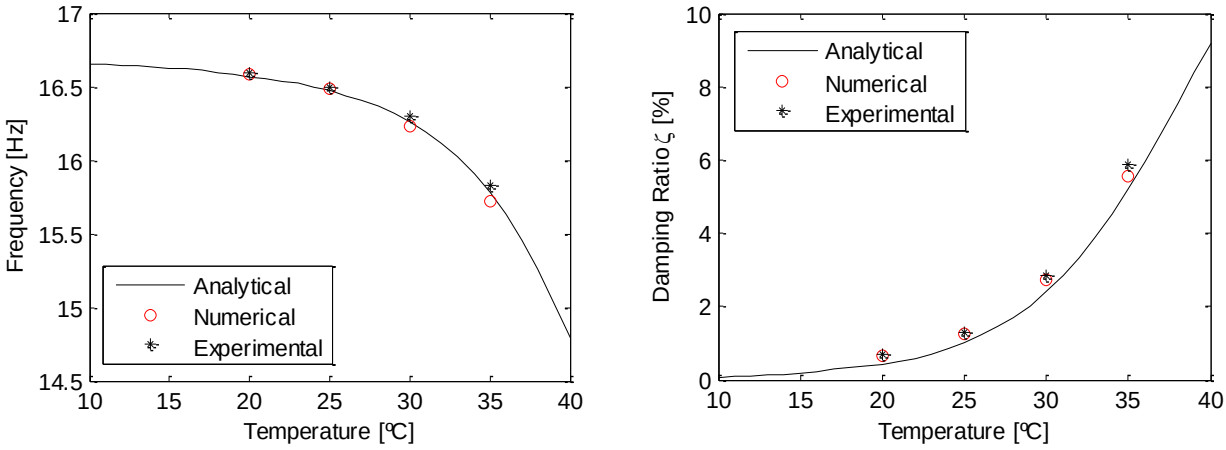

Figure 10. Analytical, numerical and experimental results for the simply-supported boundary conditions: Mode 1.

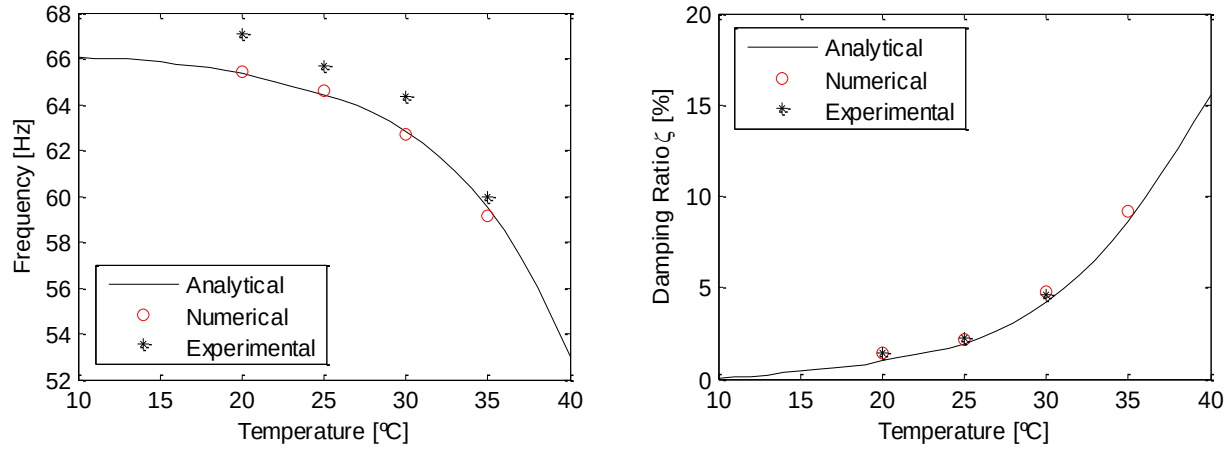

Figure 11. Analytical, numerical and experimental results for the simply-supported boundary conditions: Mode 2.

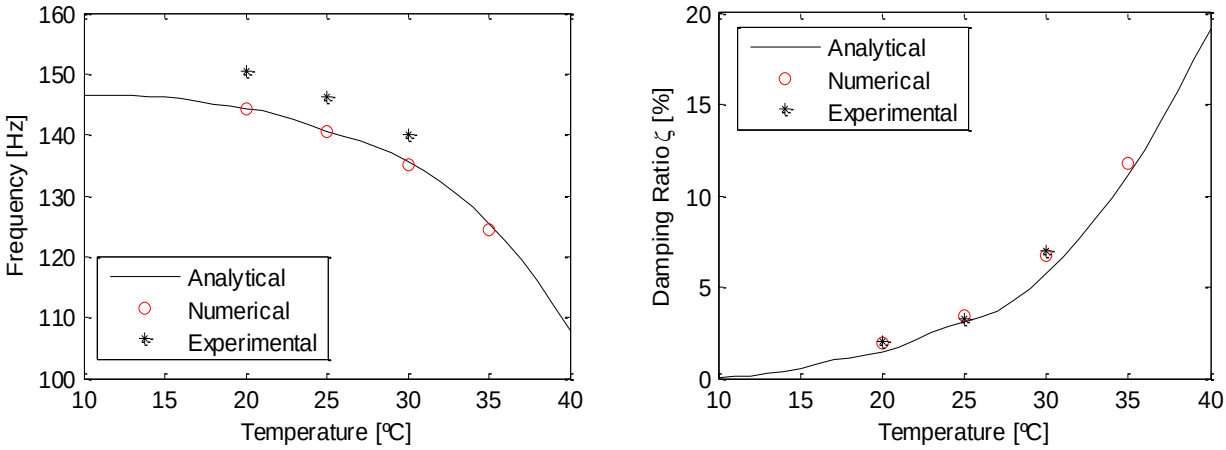

Figure 12. Analytical, numerical and experimental results for the simply-supported boundary conditions: Mode 3.

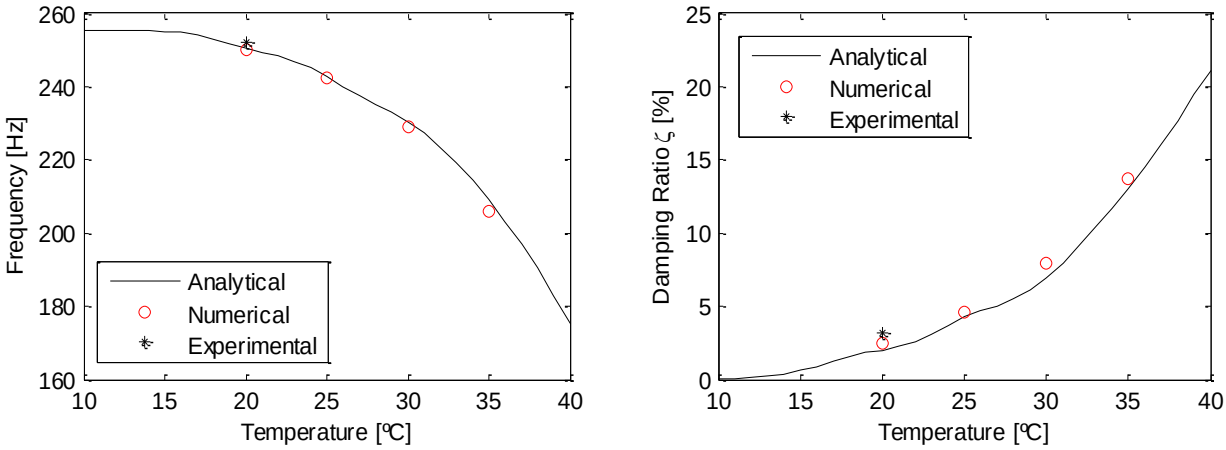

Figure 13. Analytical, numerical and experimental results for the simply-supported boundary conditions: Mode 4.

Discussion of the results

The mechanical properties of PVB undergo a radical change at a point that is referred as the glass transition temperature [15]. Below this temperature PVB presents a solid elastic-like behaviour (stiffer) and the mechanical behaviour of the laminated glass beam is close to that of a monolithic one, i.e. the beam exhibits high stiffness and low damping. At temperatures about the glass transition temperature, PVB stiffness decreases with increasing temperature [15] and a laminated glass beam exhibits lower stiffness and higher damping.

The mechanical properties of PVB vary with the percentage of plasticizer used in the manufacturing [47] Pure PVB has a transition temperature of 70^oC but this temperature decreases with increasing percentage of plasticizer (percentage which depends on the manufacturer). This aforementioned behaviour can be observed from Figs. 6 to 13. Below 20^oC the predicted natural frequencies are approximately constant and the predicted damping is low. Over the transition temperature the natural frequencies decrease with temperature and the damping increases. It can also be observed in the figures that the numerical and the experimental natural frequencies and damping ratios follow the same tendency as those predicted with the analytical model.

It can be observed in tables 4 and 5 that the discrepancies between the analytical and the numerical natural frequencies are consistently less than 2% for both simply-supported and free-free boundary conditions in all the temperature range considered in the investigation.

The discrepancies between the experimental natural frequencies and those predicted with the analytical and the numerical models are less than 5% (see tables 4 and 5), which confirm that Eq. (27) predicts with a good accuracy the natural frequencies of a multi-layered glass beam.

It can also be inferred from tables 4 and 5 that the experimental natural frequencies are always slightly lower than those predicted with the RKU model (Eq. (27)) for the free-free boundary conditions. This is in agreement with previous results obtained by the authors [18] in free-free beams composed of two layers and one PVB interlayer. On the other hand, the experimental natural frequencies of the simply-supported beam are slightly higher than the analytical ones predicted with the RKU model.

With respect to the damping ratios, it is known from statistical theory that the uncertainty bounds of damping ratios are much higher than those of the natural frequencies [41, 42 and 40]. The discrepancies between the damping ratios provided by the analytical and the numerical models are less than 40% for both boundary conditions (see tables 4 and 5). In the simply-supported boundary condition the numerical damping ratios are consistently higher than those provided by the analytical model whereas they are always less than the analytical ones in the free-free boundary condition.

With regard to the experimental damping ratios, the maximum discrepancies between the numerical and the analytical damping ratios are less than 50% (see tables 4 and 5). Again, the experimental damping ratios of the simply-supported beam are higher than the

analytical ones whereas they (the experimental ones) are lower in the free-free configuration. These results are in agreement (similar level of error) with those obtained by the authors [18, 19] in free-free beams composed of two layers and one PVB interlayer.

Conclusions

In recent years the effective thickness concept has become a simple and useful technique to estimate stresses, displacements and modal parameters in laminated glass beams and plates. In this paper expressions for the dynamic effective thickness and the dynamic effective Young modulus corresponding to a multi-layered glass beam have been derived from the static effective thickness developed by Galuppi and Royer-Carfagni [5] using the correspondence principle [13, 14, 39, 40].

These expressions can be used to determine modal parameters in multilayered laminated glass beams. The predicted modal parameters can be utilized in preliminary calculations, validation of numerical simulations and of experimental results as well as to calculate displacements and stresses [37]. The equations are easy to use and easy to implement in computer programs.

The analytical expressions proposed in this paper have been used to predict the modal parameters of a multi-layered glass beam composed of three glass layers and two polymeric interlayers. In order to validate the analytical predictions, operational experimental modal tests were carried out on the beam simply-supported and with free-free configuration in the temperature range 20-35ºC. Moreover, a finite element model was assembled in ABAQUS [35] using 3D quadratic shell continuum elements for the glass layers and 3D quadratic solid hexahedral elements for the PVB layers.

Below the PVB transition temperature, the beam exhibits a constant high stiffness and low damping and over this temperature the damping increases significantly and the natural frequencies decrease with increasing temperature. This effect can be observed in figures from 6 to 13, where both the analytical and numerical predictions follow the same tendency as the experimental results .

The discrepancies in natural frequencies between the analytical predictions and those obtained with the numerical model are less than 2% for all the modes in the temperature range considered in the investigation. With respect to the discrepancies between the experimental natural frequencies, estimated with operational modal analysis, and those provided by the analytical equations and the numerical model are consistently less than 5%.

With regard to the damping ratios, the uncertainty bounds of damping ratios are much higher than those of the natural frequencies [46]. The discrepancies between the

numerical and the analytical predicted damping ratios are consistently less than 40% whereas the maximum discrepancies between the experimental damping ratios and those predicted with the analytical and the numerical models are less than 50%. This level of discrepancy is similar to that obtained by the authors in previous works. [18, 19].

Acknowledgments

The financing support given by the Spanish Ministry of Economy and Competitiveness through the project BIA2014-53774-R is gratefully appreciated.

References

1. Galuppi L and Royer-Carfagni GF. Laminated Beams with Viscoelastic Interlayer. *J Solids Struct* 2012; 49(18): 2637-2645.

2. Galuppi L and Royer-Carfagni GF. Effective Thickness of Laminated Glass Beams: New Expression via a Variational Approach. *Eng Struct* 2012; 44:53-67.

3. Calderone I, Davies PS and Benninson SJ. Effective Laminate Thickness for the Design of Laminated Glass. In: *Glass Processing Days*, Tampere. Finland, 2009.

4. Bennison SJ, Qin M and Davies P. High-performance laminated glass for structurally efficient glazing. *Innovative light-weight structures and sustainable facades*, Hong Kong, 2008.

5. Galuppi L and Royer-Carfagni GF. Enhanced Effective Thickness of Multi-Layered Laminated Glass. *Compos Part B-Eng* 2014; 64:202-213.

6. Bennison SJ and Surreis F. Designing the Grand Canyon's new laminated glass walkway. In: *Glass Processing Days*, Tampere. Finland, 2007.

7. Feldmann M, Kasper R et al. Guidance for European Structural Design of Glass Components. *JCR Scientific and Policy Report*. 2014; doi: 10.2788/5523.

8. Haldimann M, Luible A and Overend M. Structural Use of Glass. *Structural Engineering Documents* (10). IABSE, 2008.

9. DIN 18008-5. Glass in Building – Design and construction rules. Part 5: Additional requirements for walk-on glazing, 2013.

10. ÖNORM B3716-5. Glass in building – Structural Glass Construction – Part 5: Point fixed Glazing and Special Structures, 2013.

11. ASTM 2751-11. Practice for the Design and Performance of Supported Glass Walkways.

12. Jones DIG. Reflections on Damping Technology at the End of the Twentieth Century. *J Sound Vib* 1996; 190(3):449-462.

13. Lee EH. Stress Analysis in Viscoelastic Bodies. *Q J Mech Appl Math* 1955; 13:183-190.

14. Read WT. Stress Analysis for Compressible Viscoelastic Materials. *J Appl Phys* 1950; 21:671-674.

15. Ferry JD. Viscoelastic Properties of Polymers, Third ed., John Wiley & Sons, Ltd., New York 1980.

16. Foraboschi P. Three-layered plate: elasticity solution. *Compos Part B-Eng* 2014; 60: 764-776.

17. Wölfel E. Nachgiebiger Verbund Eine Näherungslösung und deren Anwendungsmöglichkeiten. In: *Stahlbau* 1987; 6:173-180.

18. López-Aenlle M and Pelayo F. Frequency Response of Laminated Glass Elements: Analytical Modelling and Effective Thickness. *Appl Mech Rev* 2013; 65(2):020802 (13 pages).

19. López-Aenlle M and Pelayo F. Dynamic effective thickness in laminated-glass beams and plates. *Compos Part B-Eng* 2014; 67:332-347.

20. Galuppi L and Royer-Carfagni GF. The Effective Thickness of Laminated Glass Plates, *J Mech Mater Structures* 2012; 7(4):375-400.

21. Kerwin EM. Damping of Flexural Waves by a Constrained Viscoelastic Layer. *J Acoust Soc Am* 1959; 31(7):952-962.

22. Ross, D., Ungar, E.E., and Kerwin, E.M. Damping of Plate Flexural Vibrations by Means of Viscoelastic Laminate. Struct. Damp. ASME. 49-88 (1959).

23. Ditaranto RA and McGraw Jr JR. Vibratory Bending of Damped Laminated Plates, *J Eng Ind* 1959; 91(4):1081-1090.

24. Ditaranto RA. Theory of Vibratory Bending for Elastic and Viscoelastic Layered Finite-Length Beams. *J Appl Mech* 1965; 32:881-886.

25. Mead DJ and Markus S. The Forced Vibration of a Three-Layer, Damped Sandwich Beam with Arbitrary Boundary Conditions. *J Sound Vib* 1969; 10(2):163-175.

26. Mead DJ and Markus S. Loss Factors and Resonant Frequencies of Encastré Damped Sandwich Beam. *J Sound Vib* 1970; 12(1):99-112.

27. Tiantang Y, Shuohui Y, Tinh QB, Shifeng X, Satoyuki T NURBS-based isogeometric analysis of bucking and free vibration problems for laminated composites plates with complicated cutouts using a new simple FSDT theory and level set method. *Thin Wall Struct* 2016: 101:141-156.

28. Shuohui Y, Tiantang Y, Tinh QB, Shifeng X and Sohichi H. A cutout isogeometric analysis for thin laminated composites plates using level sets. *Compos Struct* 2015: 127: 152-164.

29. Tinh QB, Minh NN and Chuanzeng Z. A moving Kriging interpolation-based element-free Galerkin method for structural dynamics analysis. *Comput Methods Appl Mech Engrg* 2011: 200:1354-1366.

30. Tinh QB, Minh NN and Chuanzeng Z. An efficient meshfree method for vibration analysis of laminated composite plates. *Comput Mech* 2011: 48: 175-193.

31. Tinh QB and Minh NN. Eigenvalue analysis of thin plate with complicated shapes by a novel mesh-free method. *Int J App Mech* 2011: 1(3): 21-46.

32. Tinh QB, Du DN, Xiaodong Z, Sohichi H and Romesh CB. Analysis of 2-dimensional transient problems for linear elastic and piezoelectric structures using consecutive-interpolation quadrilateral element (CQ4). *Eur J Mech A/Solids* 2016: 58: 112-130.

33. Tschoegl NW. The phenomenological theory of linear viscoelastic behaviour.

Berlin: Springer-Verlag, 1989.

34. Lakes RS. Viscoelastic materials. Cambridge: Cambridge University Press, 2009.

35. Abaqus User's Manual, Dassault Systémes Simulia Corp., Providence, Rhode Island, USA.

36. Rao DK. Frequency and loss factors of sandwich beams under various boundary conditions. *J. Mech Eng Sci* 1978; 20(5):271-282.

37. López-Aenlle M, Pelayo F and Ismael G. An effective thickness to estimate stresses in laminated glass beams under dynamic loadings. *Compos Part B-Eng* 2015; 82:1-12.

38. López-Aenlle M and Pelayo F. Dynamic effective thickness in laminated-glass beams and plates. *Compos PartB-Eng* 2014; 67:332-347.

39. Kimberly JB. Design and Analysis of Constrained Layer Damping Treatments for Bending and Torsion, Ph.D Thesis. Ohio: Air Force Institute of Technology, 1994.

40. Williams ML, Landel RF and Ferry J. The Temperature Dependence of Relaxation Mechanisms in Amorphous Polymers and Other Glass-forming Liquids. *J Amer Chem Soc* 1955; **77:**3701-3707.

41. Ewins DJ. Modal Testing: theory, practice and application (2nd Ed.). John Wiley & Sons Ltd. 2000.

42. Maia MM, Silva MM et al. Theoretical and Experimental Modal Analysis. Research Studies Press and John Wiley & Sons Ltd. 2007.

43. Fröling M and Persson K. Computational Methods for Laminated Glass. *J. Eng. Mech*. 2013; 10.1061/(ASCE)EM.1943-7889.0000527. pp. 780-790.

44. Brincker R, Zhang L-M and Anderson P. Modal Identification from Ambient Response Using Frequency Domain Decomposition. In: *Proceedings of the 18th IMAC*, pp. 625-630, 2000.

45. Van Overschee P and De Moor B. Subspace Identification for Linear Systems: Theory, Implementation & Applications. Dordrecht, Netherlands, Kluwer Academic Publishers, 1996.

46. Gersch W. On the Achievable Accuracy of Structural System Parameter Estimates. *J Sound Vib* 1974; 34(1):63-79.

47. López-Anido RA and Naik TR. Emerging materials for civil infrastructure: state of the art. ASCE Publications 2000.